

A conceptual design of an electron spectrometer for ELI-NP

S. Balascuta and I. C. E. Turcu

Citation: [AIP Conference Proceedings](#) **1645**, 296 (2015); doi: 10.1063/1.4909589

View online: <http://dx.doi.org/10.1063/1.4909589>

View Table of Contents: <http://scitation.aip.org/content/aip/proceeding/aipcp/1645?ver=pdfcov>

Published by the [AIP Publishing](#)

Articles you may be interested in

[Cryogenic stopping cell for photofission fragments at the ELI-NP facility](#)

AIP Conf. Proc. **1681**, 030002 (2015); 10.1063/1.4932246

[Positron production at extreme light infrastructure – nuclear physics \(ELI-NP\)](#)

AIP Conf. Proc. **1645**, 372 (2015); 10.1063/1.4909604

[Gamma beam system at ELI-NP](#)

AIP Conf. Proc. **1645**, 237 (2015); 10.1063/1.4909580

[Perspectives for neutron and gamma spectroscopy in high power laser driven experiments at ELI-NP](#)

AIP Conf. Proc. **1645**, 228 (2015); 10.1063/1.4909579

[High power femtosecond lasers at ELI-NP](#)

AIP Conf. Proc. **1645**, 219 (2015); 10.1063/1.4909578

A Conceptual Design of an Electron Spectrometer for ELI-NP

S. Balascuta^{1, a)}, I. C. E. Turcu¹

¹National Institute for Physics and Nuclear Engineering, ELI-NP, Str. Reactorului, nr. 30, P.O.Box MG-6, Bucharest-Magurele, Romania

^{a)}Corresponding author: Septimiu.Balascuta@eli-np.ro

Abstract. We present the geometry and field parameters of an Electron Spectrometer (ES) with two dipole magnets, considered for electron energy measurements at the High Fields QED experimental area at ELI-NP. The first magnet is a 2 meter long permanent magnet, placed inside the Interaction Chamber (IC). The second magnet is a 1.5 meters long electromagnet, placed outside IC. The pulsed electron beam will be produced by the 10 PW pulsed Laser, ‘pump-beam’, focused into one meter long capillary low density plasma cell. A second 10 PW pulsed Laser, ‘probe-beam’, will interact with the relativistic electron bunch providing the strong electromagnetic field. The ES will measure the subtle changes in the electron energy spectrum as a result of the electron beam interaction with the probe-beam field.

1. Introduction

At the High Fields QED experiments proposed at ELI-NP [1,2,3] the two 10 PW Laser beams will be focused on solid or gas targets. For the gas target experiments, a pulsed Laser (pump) beam is focused with the F/20 parabolic mirror in a long capillary cell (Fig.1) to produce and accelerate bunches of electrons through the wakefield acceleration in plasma [4]. At the exit of the capillary the electrons interact with a second (probe) Laser beam focused with the F/3 parabolic mirror. The intensity of the probe in the focus has to be between 10^{22} and 10^{23} W/cm² to assure that the normalized transverse vector momentum of the laser field $a_0 = eA/mc^2$ is much bigger than one. The electrons gains a longitudinal drift momentum proportional with a_0^2 that can be significant if the probe beam is opposite to the direction of the electron bunch. In such strong fields the radiation reaction force is equal or even exceeds the applied force of the Laser field. The experiment can potentially study the radiation reaction force and the non-linear Compton effect. The radiation reaction was studied with the Lorentz-Abraham-Dirac equation [5] but also through perturbative [6] or non-perturbative [7] approaches and is the subject of recent experiments [8].

In a previous experiment [9], the energy spectrum of a wakefield accelerated electron beam was measured with a 40 cm long electromagnet. Because at ELI-NP, the electron energy is expected to exceed 10 GeV, a permanent magnet (2 m long) followed by an electromagnet (1.5 m long) was suggested for such measurements (Fig.1). The energy resolution $\Delta E/E$ of the Electron Spectrometer, depends on the electron energy, the magnetic flux intensity, the length and the high of the gap located between the two magnets. We calculated the relative energy lost $\Delta E/E=20\%$ of electron beam due to the nonlinear Thomson scattering [10] of a pulsed laser beam (with 25 fs/pulse and 10^{22} W/cm²). Therefore an energy resolution $\Delta E/E$ better than 10% should be sufficient to resolve the fine changes in the electron-energy spectrum due to ‘radiation-reaction’ and other strong fields effects.

The electrons with high enough energy exit through the vertical face of the permanent magnet, enter in the gap of a 1.5 meter long electromagnet and interacts with the Lanex Scintillating Screens (SS) located outside the IC. The light emitted from the electron spot on the SS is detected by CCD cameras located on the lateral or the top walls of the IC.

Considering a uniform magnetic field in the gap volume delimited by the two poles (Fig.2) the smallest width (G) of the gap, required for the electrons to exit the magnet without interacting with the lateral walls, is

related to the length L of the gap, the divergence of the electron beam (α), the uncertainty in the position of the entrance point of the beam $\pm dx$ and in the angle (θ) between the incoming electron beam direction and Z axis.

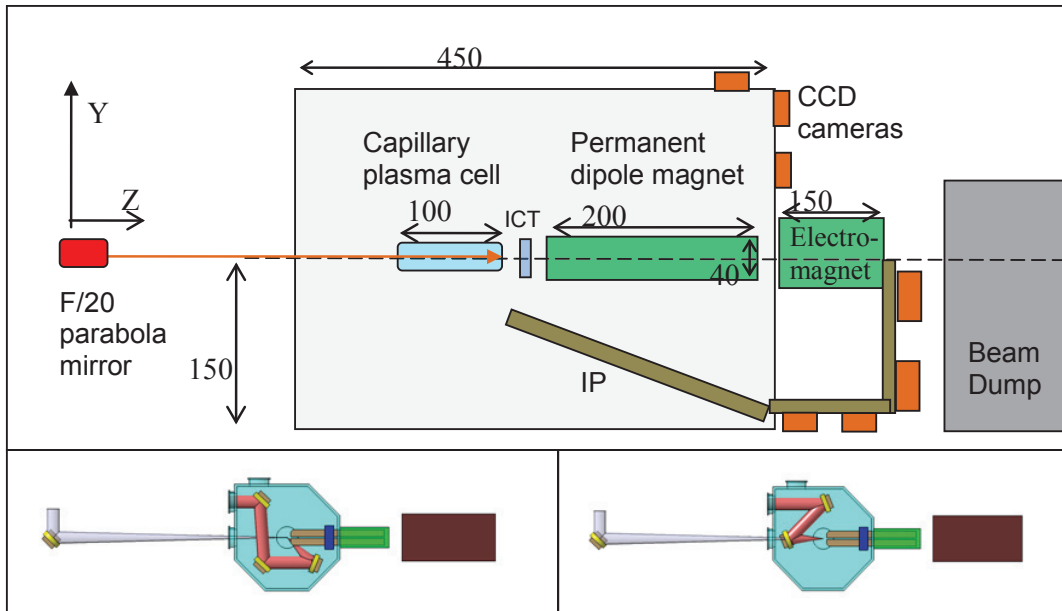


FIGURE 1. A projected view in the vertical plane through the Laser beam axis, of the interaction chamber, capillary plasma cell, Integrated Charge Transformer (ICT), permanent magnet, electromagnet, scintillating screens (SS) with CCDs, and beam dump (top figure). The two bottom figures are two laser beams configurations proposed for the experimental area E6 (High Fields QED) at ELI-NP. The two 10 PW laser beams make a 135° angle (left figure) or a 0° angle (right figure).

The angle θ varies from shot to shot due to the electron transverse momentum acquired during acceleration.

$$G = dx + 2L \tan(\theta + \alpha) \quad 1)$$

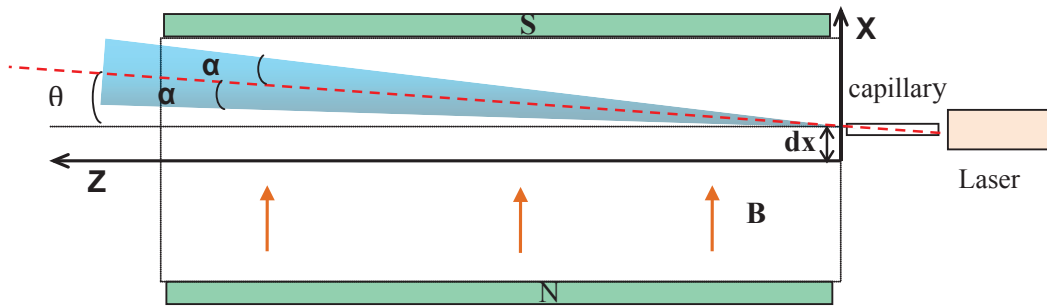


FIGURE 2. The geometry of the magnet gap is projected in the horizontal plane (XZ) passing through the center of the magnet and the Z axis, that is the axis of symmetry for the magnet poles. The direction of the electron beam axis is in the XZ plane and makes the angle θ with the Z axis. The trajectories of the electrons emitted from the capillary cell are located inside the cone with opening angle α (the triangular filled area).

The expected uncertainty dx is 0.1 cm. The angular uncertainty in the electron beam axis $\theta = 0.02$ rad and the electron beam divergence $\alpha = 0.005$ rad [9]. The suggested modular Electron Spectrometer is made from a permanent magnet (section 2) and an electromagnet (section 3). The precision in energy measurement is calculated in section 4.

2. The Permanent Magnet

The geometry of the fixed dipole magnet with NdFeB magnets and cylindrical Iron yoke is presented in Fig.3a. The Iron yoke is the cylinder that surrounds all the pairs of permanent magnets except at the bottom

where the rectangular slit allows the electrons (with energy less than 1 GeV) to exit the magnet and interact with the SS on the bottom of the IC. The orientation of the magnetization in each magnet is indicated with red arrows. The gap is $G = d_1 \cos(75^\circ)$ where “ d_1 ” is the diameter of the two pole magnets. The ratios of the three diameters are $d_2/d_1=1.5$, $d_3/d_1=2.2$ and the opening angle for each lateral magnet is 30° . The mass of the $L=4$ m long magnet with $G=20.1$ cm, $d_1=77.65$ cm, $d_2=116.48$ cm, $d_3=170.85$ cm, is $m_1 = \rho_{NdFeB} \cdot (\pi \cdot d_2^2/4 - G \cdot d_2)L + \rho_{Fe} \cdot [\pi(d_3^2 - d_2^2)/4 - G(d_3 - d_2)/2]L = 61.64$ tons. The mass of a 2 m long permanent magnet with $G=10.1$ cm, $d_1=39$ cm, $d_2=58.6$ cm, $d_3=85.8$ cm is $m_2=7.8$ tons. The field calculations were done with a Comsol 2D model of the magnet width gap widths from 1 cm to 10 cm, keeping the ratios G/d_1 , d_2/d_1 , d_3/d_1 and the remnant magnetic flux (1.3 Tesla for NdFeB) fixed. The total magnetic flux in the center of the magnet was 1.1 Tesla for all gap widths considered. The magnetic field calculated along the Y axis (Fig.3b) was used to compute the electron trajectory in the YZ plane.

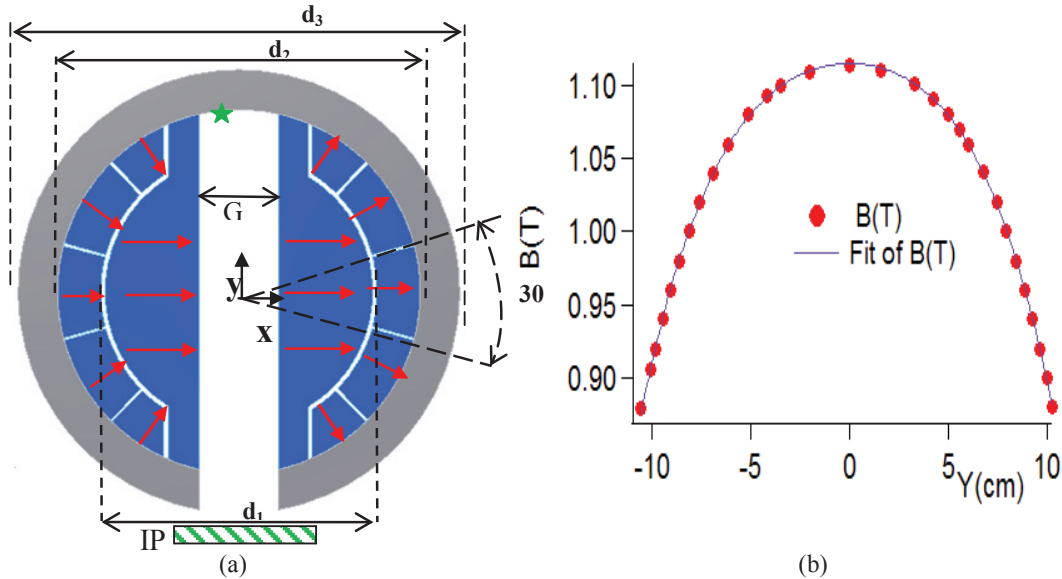


FIGURE 3: A) The geometry of the magnet is presented in the vertical plane (XY) normal to the axis of the Laser beam (Z axis). B) The map of the magnetic flux density in the circular dipole magnet with permanent magnets and cylindrical Iron Yoke, is presented in the vertical plane XY normal to the Laser beam axis (that is the Z axis).

The 200 cm long magnet (with its transversal cross section presented in Fig. 3) has a 58.5 cm high gap. The point where the electron beam enters that Gap is marked with a star in Fig. 3. Because the resolution power of the fixed dipole magnet depends on the length of the electron trajectory in the field, it is necessary that the Laser beam enters the cylindrical magnet, close to the top of the gap but below the Iron shield.

3. The Electromagnet

The magnetic flux density on the surface of the Comsol model for the electromagnet and the field calculated along vertical axis are presented in Fig. 4. The “C” Iron yoke provides the return flux for the magnetic field. The electromagnet has two solenoids with copper coils cooled with water. The origin of the axis is in the center of the gap. The gap width for the electromagnet is $G=7.6$ cm and the gap height is 30 cm.

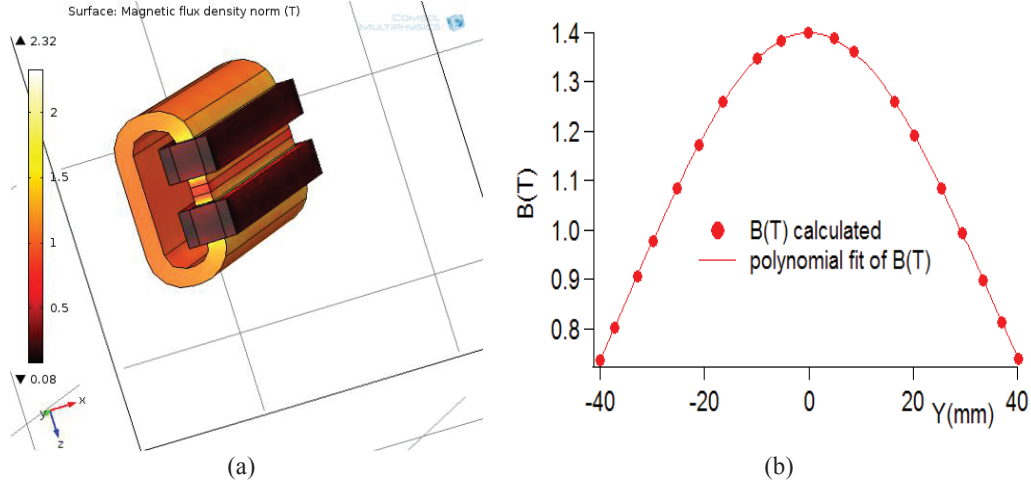


FIGURE 4: In the left figure the surface magnetic flux density $B(T)$ is calculated for the 1.5 meter long electromagnet. The right figure presents the magnetic flux density calculated along the vertical direction (Y) passing through the center of the gap and a fourth order polynomial fitting function.

4. The Precision in Energy Measurement

The magnetic field of the first magnet built from NdFeB permanent magnets does not change when the strong Electromagnetic Pulse is emitted upon the LASER beam interaction with the target. We consider that the electron bunches enters parallel with the Z axis, uniform B field confined inside the gap and θ the tilt angle of the electron momentum when the electron exit the field region. The vertical displacement of the electron bunch, measured on the exit face of the magnet, is given by equation 2, where R and L are the radius of electron trajectory (in the magnetic field) and the length of the magnet respectively:

$$y = R(1 - \cos \theta) = R - \sqrt{R^2 - L^2} \quad (2)$$

The radius depends on the electron energy (E) and on the magnetic field $R = mc^2 \sqrt{\gamma^2 - 1} / (qBc)$ where $\gamma = E/mc^2$. Therefore the change in the vertical displacement of the electron bunch center divided with the small change in its energy is equal with:

$$\frac{dy}{dE} = \frac{dR}{dE} \left(1 - \frac{R}{\sqrt{R^2 - L^2}} \right) = \frac{\gamma}{qBc} \left(\frac{1}{\sqrt{\gamma^2 - 1}} - \frac{1}{\sqrt{\gamma^2 - 1} - (qBcL)^2 / (mc^2)^2} \right) \quad (3)$$

The magnetic field of the electromagnet is $B_2 = 1.5T$. The radii of the trajectories for an electron moving in the magnetic fields B_1 and B_2 are R_1 and R_2 respectively. The vertical displacement of the electron bunch after passing through the fields of the two magnets is equal with the sum of the two vertical displacements due to each magnet:

$$y_{1,2} = \left(R_1 - \sqrt{R_1^2 - L_1^2} \right) + R_2 \left(\sqrt{1 - L_1^2/R_1^2} - \sqrt{1 - (L_1/R_1 + L_2/R_2)^2} \right) \quad (4)$$

The diameter of the electron bunch when it enters in the field is less than 0.5 mm. After passing through electromagnet the diameter of the electron spot is between 1 and 2 mm due to the Coulomb interaction between electrons. Two electron-beam spots with energies E and $E-dE$ can still be resolved, if the distance between their centers is bigger or equal with the diameter of a spot. The energy derivative of the displacement ($T=dY_{1,2}/dE$) was calculated from equation 4. In Fig. 4, the relative energy uncertainty $dE/E = -\Delta Y_{1,2}/(T \cdot E)$ is calculated for electrons with energy E (spot diameter $d = -\Delta Y_{1,2}$), for a 4 m long magnet (with $B=1$ T) and for the assembly of two magnets. In the last case, the energy resolution for 38 GeV electrons is 1.75% if $d=1$ mm or 3.5% if $d=2$ mm. Fig. 5a presents the relative error in the electron bunch energy (with 1 or 2 mm diameter spot).

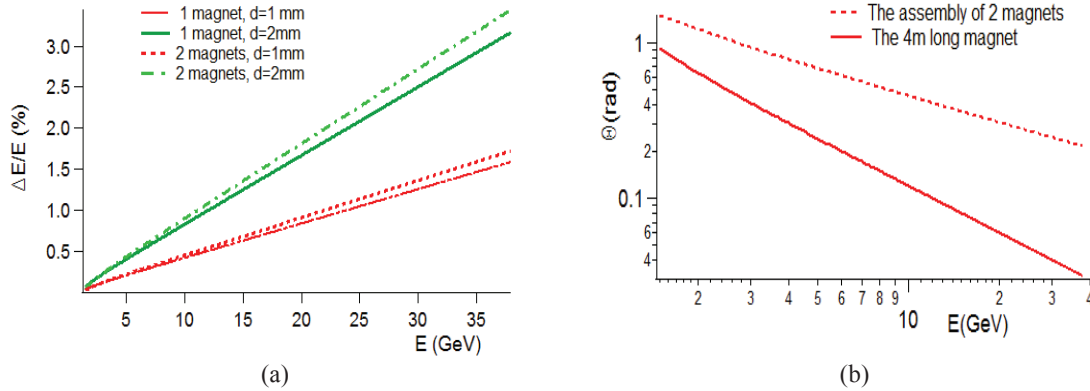


FIGURE.5: a) The calculated relative error expected in the energy measurement of an electron bunch (with diameter “d”) on the vertical LS is calculated for 1 magnet (5 m long, d=2 mm, solid line) and for assembly of two magnets ($L_1=2$ m , $L_2=1,5$ m, d=1 or 2 mm, dotted line) versus the electron beam energy b) The angle θ between the direction of the electron momentum and the Z axis, at the exit of the 4 m long permanent magnet or of the assembly of two magnets is calculated for electrons with energies 1.5 GeV to 38 GeV.

5. Conclusion

The gap width depends on the angular dispersion of the electron beam at its entrance in the field. Considering the angular dispersion in the electron beam axis of 0.02 radians and the longitudinal and intrinsic energy dispersion, the expected uncertainty in energy measurement is between 5% and 10%. Because the diameter of the electron bunch increases with the length of the electron trajectory, the spot diameter is smaller for the assembly of two magnets than for a 4 m long magnet. A 1 meter long superconducting magnet, with a peak field of 6 T, can provide the same energy resolution like a 4 m long magnet. However such a magnet exceeds the budget and can be damaged by the electromagnetic pulses generated upon the laser interaction with the target.

ACKNOWLEDGMENTS

We had useful discussions with Florin Negoita , Ioan Dancus, Mihail Cernaianu and Daniel Ursescu who proposed the modular geometry of the Electron Spectrometer based on a permanent magnet and an electromagnet. Thanks to Matei Tataru, Mihai Risca and Cristian Petcu for their 3D modeling of the Laser beam configuration in the E6 interaction chamber. We thank Professor Dino Jaroszynski and the ELI-NP working group for the experimental configurations with solid and gas targets and valuable comments.

REFERENCES

1. N.V. Zamfir et al., *Extreme Light Infrastructure: nuclear physics*, Proc. SPIE, 8080, (2011), pp. 80800X-1
2. O. Tesileanu et al., *Extreme Light Infrastructure-Nuclear Physics*, Journal of Physics- Conference Series, 420 (2013) pp. 12157
3. D. Ursescu et al., *The Review of Laser Engineering*, **42** (2), 123 (2014)
4. E. Esarey, C. B. Schroeder, W. P. Lemans, *Rev. of modern phys.*, **81**,1229- 1230 (2009) .
5. P. A. M Dirac, *Proc. R. Soc. Lond. A*, **167**, 148 (1938).
6. L. D. Landau, E. M. Lifshitz, *Classical Theory of Fields* , 4th ed. Butterworth –Heinemann (Linacre House, Oxford, 2000)
7. W. Ford , R. F. O’Connell, *Phys. Lett. A* **157**, 217 (1991)
8. N. Neitz, A. Di Piazza , *Phys. Rev. Letters*, **111**, 054802 (2013)
9. K. Nakamura et al., *Review of Scientific Instruments*, **79**, 053301, (2008)
10. E. Esary et al. *Phys. Rev. E*, **48**, 3003, (1993)